

Photophysics of Perylene Monoimide-labelled Organocatalysts

Dongdong Zheng, Mina Raeisolsadati Oskouei, Hans J. Sanders, Junhong Qian, René M. Williams, and Albert M. Brouwer*

Electronic Supporting information

Contents

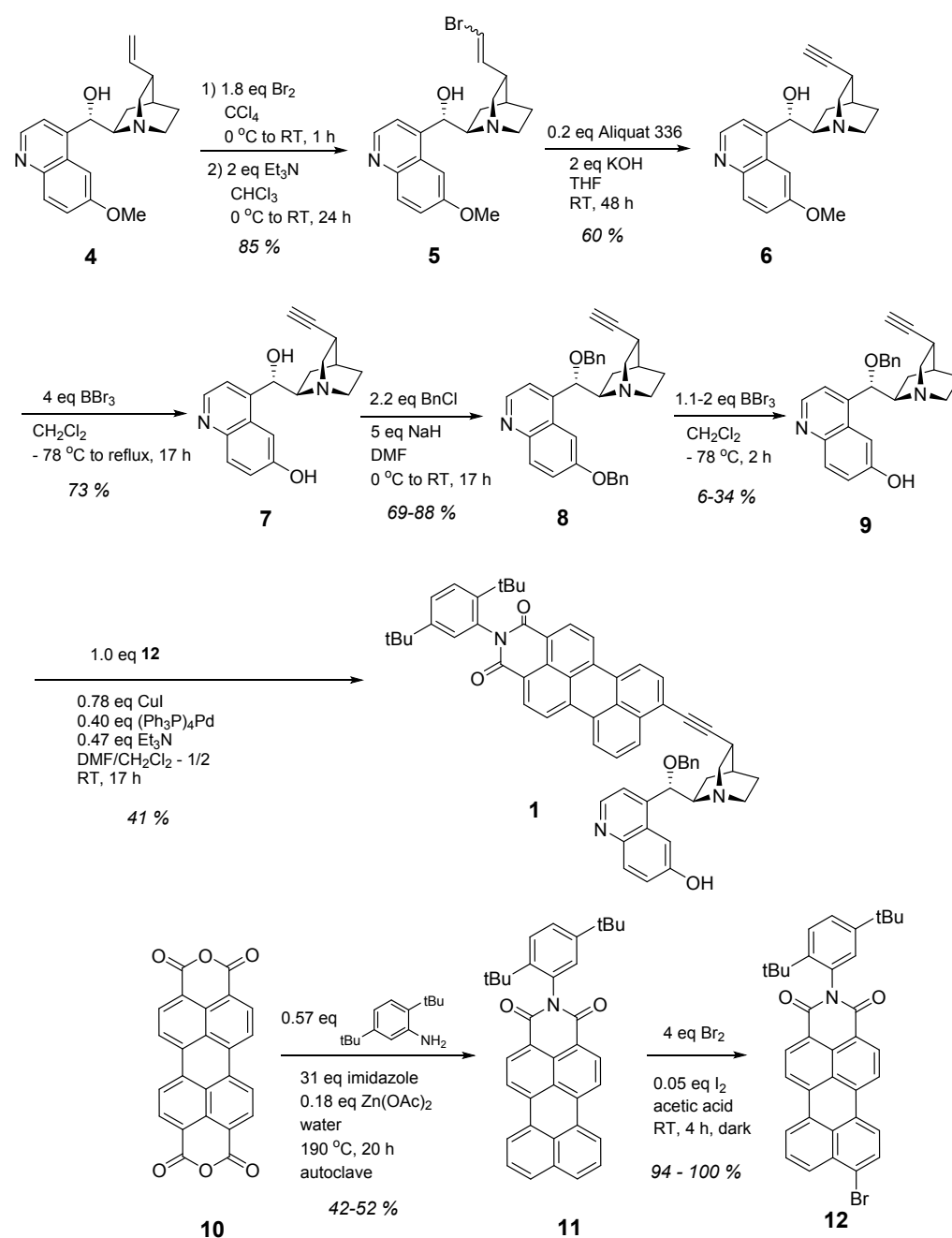
1	Syntheses	S2
1.1	Synthesis of PMI-BnCPD 1	S2
1.2	Synthesis of PMI-dHQD 2	S4
2	Other materials	S5
3	HPLC analysis of PMI-BnCPD 1	S6
4	Spectroscopic measurements	S7
4.1	Absorption and fluorescence spectra	S7
4.2	Fluorescence Lifetime	S7
4.3	Femtosecond Transient Absorption (fsTA)	S7
4.4	Additional spectra and fluorescence decay curves	S8
5	Cyclic voltammogram of quinuclidine, the model electron donor	S11
6	Additional fsTA spectra	S12
7	Conformational analysis	S13
8	NMR spectra	S14
9	LCMS analysis of compound 1	S19
10	References	S20

1 Syntheses

The synthesis of compounds **6** and **7** starting from commercially available quinidine **4** followed the methods of Marcelli.¹ The starting compound **12** was prepared as described in reference 2. Compounds **1** and **2** were prepared by Sonogashira coupling of **12** to **9** and **6**, respectively.

All experiments were performed under a nitrogen atmosphere, unless stated otherwise.

1.1 Synthesis of PMI-BnCPD 1



Scheme S1. Synthesis of PMI-BnCPD, compound **1**.

(1S,2R,4S,5S)-2-((S)-(benzyloxy)(6-(benzyloxy)quinolin-4-yl)methyl)-5-ethynylquinuclidine (8). To a cooled (0 °C) solution of **7** (2.81 g, 9.1 mmol) in 100 ml dry DMF was added NaH (1.82 g of a 60 % dispersion in mineral oil, 45.6 mmol), after which the resulting mixture was stirred for 1 h at RT. Next, benzylchloride (2.30 ml, 2.53 g, 20.0 mmol) was added, after which the reaction mixture was stirred 17 h at RT. Conversion was checked by TLC and found to be complete. The reaction mixture was quenched with 50 ml water, diluted with 1 L EtOAc and washed 4 × 100 ml water. The organic layer was dried (Na₂SO₄) and concentrated in vacuo to give an oily biphasic product. This was dissolved again in 500 ml EtOAc, which was washed with 3 × 100 ml water and 100 ml brine, dried (Na₂SO₄) and concentrated in vacuo to give 4.59 g. This was flash chromatographed (SiO₂, gradient CH₂Cl₂/MeOH – 99/1 → 98.5/1.5 → 98/2 → 97/3) to afford 3.06 g of **5** (yield 69 %) as a brown oil. ¹H NMR (400 MHz, CDCl₃) δ 8.76 (d, *J* = 4.5 Hz, 1H), 8.07 (d, *J* = 9.2 Hz, 1H), 7.54 (bs, 1H), 7.51 – 7.27 (m, 12H), 5.15 (m, 3H), 4.48 – 4.30 (m, 2H), 3.31 - 3.23 (m, 1H), 3.09 (q, *J* = 8.4 Hz, 1H), 2.93 (dd, *J* = 13.4, 10.5 Hz, 1H), 2.61 - 2.54 (m, 2H), 2.51 – 2.40 (m, 1H), 2.31 – 2.26 (m, 1H), 2.07 (d, *J* = 2.4 Hz, 1H), 1.97 (bs, 1H), 1.59 - 1.39 (m, 3H); TLC : R_f ≈ 0.6 (CH₂Cl₂/MeOH/28 % NH₄OH – 90/10/1).

4-((S)-(benzyloxy)((1S,2R,4S,5S)-5-ethynylquinuclidin-2-yl)methyl)quinolin-6-ol (9). To a cooled (-78 °C) solution of **8** (3.03 g, 6.2 mmol) in dry CH₂Cl₂ (100 ml) was added BBr₃ (6.2 ml of a 1.0 M solution in hexanes, 6.2 mmol), and the reaction mixture was stirred at -78 °C for 1 h. Another 6.2 ml of BBr₃ in hexanes was added and the reaction mixture was stirred at -78 °C for an additional 45 min. Conversion was found to be sufficiently complete. The reaction was quenched by adding 10 ml MeOH. After this the pH was adjusted to ca. 7 by adding saturated aqueous sodium bicarbonate, phosphate buffer (pH ca. 7) and 50 ml water. The layers were separated and the aqueous layer was extracted with 2 × 50 ml CH₂Cl₂. The combined organic layers were dried (Na₂SO₄) and concentrated in vacuo to give 5.58 g, which was flash chromatographed (SiO₂, gradient CH₂Cl₂/MeOH/28 % NH₄OH – 99/1/0.1 → 98.5/1.5/0.15 → 98/2/0.2 → 97/3/0.3 → 96/4/0.4 → 95/5/0.5) to give an impure product that was flash chromatographed again (SiO₂, gradient CH₂Cl₂/ MeOH/ 28 % NH₄OH – 99/1/0.1 → 98.5/1.5/0.15 → 98/2/0.2 → 97.5/2.5/0.25 → 97/3/0.3) to give a partly pure product. The mixed fractions were finally purified with preparative TLC (SiO₂, 20 × 20 cm, 1 mm thickness, CH₂Cl₂/ MeOH/28 % NH₄OH – 90/10/1) to give 0.153 g of **6** (yield 6 %) as a faint yellow resin. ¹H NMR (400 MHz, CDCl₃) δ 8.69 (d, *J* = 4.5 Hz, 1H), 8.02 (d, *J* = 9.1 Hz, 1H), 7.71 (bs, 1H), 7.54 – 7.22 (m, 7H), 5.48 (bs, 1H), 4.44 - 4.38 (m, 2H), 3.71 (bs, 1H), 3.21 - 3.08 (m, 2H), 2.95 - 2.83 (m, 1H), 2.74 - 2.66 (m, 1H), 2.57 - 2.45 (m, 2H), 2.07 (d, *J* = 2.4 Hz, 1H), 2.01 (bs, 1H), 1.58 – 1.38 (m, 2H), 1.35 - 1.26 (m, 1H); TLC : R_f ≈ 0.6 (CH₂Cl₂/ MeOH/ 28 % NH₄OH – 90/10/1).

8-(((1S,3S,4S,6R)-6-((S)-(benzyloxy)(6-hydroxyquinolin-4-yl)methyl)quinuclidin-3-yl)ethynyl)-2-(2,5-di-tert-butylphenyl)-1H-benzo[5,10]anthra[2,1,9-def]isoquinoline-1,3(2H)-dione (1). To a solution of **9** (0.153 g, 0.384 mmol) in 6.7 ml DMF and 13.3 ml CH₂Cl₂ was added 8-bromo-2-(2,5-di-tert-butylphenyl)-1H-benzo[5,10]-anthra[2,1,9-def]isoquinoline-1,3(2H)-dione **12** (0.226 g, 0.384 mmol) and triethylamine (25.1 μ L, 18.3 mg, 0.180 mmol), after which the mixture was degassed for ca. 15 min, by bubbling argon through. Next, copper(I) iodide (57 mg, 0.30 mmol) and Pd(PPh₃)₄ (0.177 g, 0.154 mmol) were added and the resulting mixture was stirred overnight at RT. Conversion was checked by means of TLC. The reaction mixture was diluted with 500 ml EtOAc and washed with 4 \times 50 ml water and 1 \times 50 ml brine. The combined aqueous layers were extracted with 200 ml EtOAc. The separations were hampered somewhat by formation of emulsions. The combined organic layers were dried (Na₂SO₄) and concentrated in vacuo. The residue (apparently still containing DMF) was dissolved in 250 ml EtOAc, washed with 3 \times 20 ml water, 1 \times 20 ml brine and again 3 \times 20 ml water and 1 \times 20 ml brine, dried (Na₂SO₄) and concentrated in vacuo to give 0.61 g, which was flash chromatographed (SiO₂, gradient CH₂Cl₂/MeOH/28 % NH₄OH – 99/1/0.1 \rightarrow 98.5/1.5/0.15 \rightarrow 98/2/0.2 \rightarrow 97.5/2.5/0.25 \rightarrow 97/3/0.3 \rightarrow 96/4/0.4 \rightarrow 95/5/0.5) to give 0.191 g of an impure product. This was purified further with preparative TLC (SiO₂, 20 \times 20 cm, 1 mm thickness, CH₂Cl₂/MeOH/28 % NH₄OH – 90/10/1) using 5 plates to give 0.144 g of **1** (yield 41 %). ¹H NMR (400 MHz, CDCl₃) δ 8.80 – 8.73 (m, 1H), 8.64 - 8.62 (m, 2H), 8.38 – 8.02 (m, 6H), 7.80 (d, *J* = 12.6 Hz, 1H), 7.63 – 7.44 (m, 5H), 7.37 (m, 1H), 7.34 – 7.27 (m, 2H), 7.08 – 6.94 (m, 4H), 5.62 (bs, 1H), 4.46 (d, *J* = 4.9 Hz, 2H), 3.95 (bs, 1H), 3.43 – 3.21 (m, 2H), 3.06 - 2.96 (m, 5H), 2.89 – 2.78 (m, 1H), 2.74 – 2.67 (m, 1H), 2.28 (bs, 1H), 1.71 – 1.56 (m, 3H), 1.36 - 1.32 (m, 18H); TLC : R_f \approx 0.4 (CH₂Cl₂/MeOH/28 % NH₄OH – 95/5/0.5).

1.2 Synthesis of PMI-dHQD 2

A round-bottomed flask was charged with dHQD **6** (ref. 2) (0.0537 g, 2.45 mmol), 9-bromo-*N*-(2,5-di-*tert*-butylphenyl)perylene-3,4-dicarboximide **12** (0.166 mmol), Pd(PPh₃)₄ (4 mg, 0.05 eq), CuI (2 mg, 0.05 eq) and 2 ml Et₃N, followed by 1 ml H₂O. The resultant mixture was stirred at 90 °C for 3.5 h, then cooled to room temperature and extracted with CHCl₃ until no red color was present in the aqueous layer. The combined organic layers were dried (Na₂SO₄) and concentrated in vacuo. Column chromatography (SiO₂, MeOH/EtOAc 1:1) afforded the coupling product PMI-dHQD as a red solid. Yield 0.052 gram (54%) of **2**.

¹H NMR (400 MHz, CDCl₃) δ = 8.67 (d, 1H), 8.43 (m, 3H), 7.94 (m, 4 H), 7.80 (dd, 1H), 7.6 (m, 2H), 7.46 (m, 3H), 7.20-7.30 (m, 2H), 7.09 (dd, 1H), 5.95 (br s, 1H), 4.01 (br s, 1H), 3.81 (s, 3H), 3.39 (m, 1H), 3.27 (m, 1H), 3.03-2.86 (m, 3H), 2.62 (t, 1H), 2.28 (m, 1H), 1.36 (s, 9H), 1.28 (s, 9H).

2 Other materials

The thiol-reactive fluorescence probe, BODIPY maleimide **3**, was synthesised according to ref. 3. All solvents were purchased from commercial chemical suppliers and were of spectroscopic or HPLC grade. The solvents showed negligible background fluorescence under the spectral conditions of the experiments. When water was used as solvent, it was of Milli-Q (Millipore) quality or doubly distilled.

3 HPLC analysis of PMI-BnCPD 1

The sample of PMI-BnCPD 1 was analyzed by means of HPLC. The mobile phase was a DCM-methanol mixture (95/5), flow speed 1 mL/min. The stationary phase was a ReproSil 150 x 4.6 mm silica column. The HPLC system consisted of Shimadzu LC-20AT and Shimadzu LC-10AT pumps, a Shimadzu DGU 14A degasser, a Shimadzu SCL-10A controller and Shimadzu SPD- M10AVP diode-array detector. Data were processed with Igor Pro.

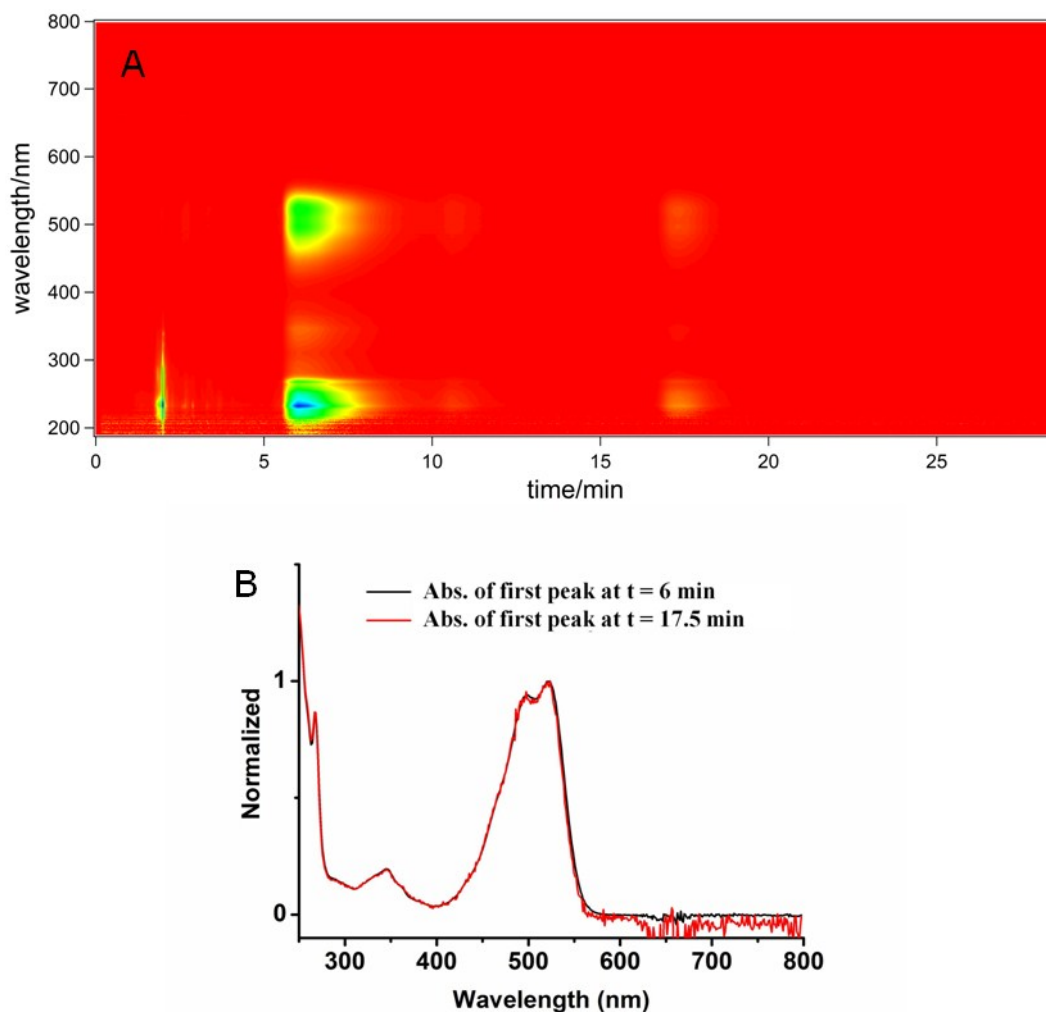


Fig. S1: A: 3D-HPLC chromatogram of compound 1 dissolved in 95% DCM/5% MeOH, where the absorption is displayed on the y-axis and the time on the x-axis. B: comparison of the normalized absorption spectra of the two compounds at elution times 6 min and 17.5 min, respectively.

By integrating the absorbances of the signals at 5-10 min and 15-20 min in the 3D HPLC chromatogram their amplitudes are found to be 97% and 3%, respectively, which are consistent with the results of the TCSPC measurements. From the spectral similarity we conclude that the impurity compound contains the same chromophore as compound 1.

4 Spectroscopic measurements

4.1 Absorption and fluorescence spectra

UV–Vis absorption spectra were measured in quartz cuvettes (1 cm, Hellma) on a Shimadzu UV2700 spectrophotometer. Fluorescence emission spectra were recorded on a SPEX Fluorolog 3 fluorimeter and are corrected for fluctuations of the excitation source flux and the wavelength dependence of the detection system. All steady-state and time-resolved measurements were done at 21°C.

4.2 Fluorescence lifetimes

Fluorescence lifetimes of PMI-BnCPD **1** and PMI-dHQD **2** were measured using time-correlated single photon counting. The detection system was described elsewhere.⁴ For excitation we used a Titanium:Sapphire laser (Chameleon Ultra-II, Coherent) with ~150 fs FWHM pulses at a repetition rate of 80 MHz. The excitation wavelength of 488 nm was obtained by frequency doubling. A pulse picker (PulseSelect, APE) was used to decrease the repetition rate of the laser from the fundamental frequency of 80 MHz to 8 MHz. TCSPC histograms were recorded using ~10⁴ counts in the peak channel. The emission wavelengths (550 and 600 nm) were selected using a Carl Zeiss M20 monochromator. A 488 nm notch filter was used to eliminate excitation light before the MCP detector (Hamamatsu R3809U-50). The decays were fitted using DecFit software^{5,6} as a sum of exponentials convolved with a measured Instrument Response Function (IRF) (FWHM ~20 ps). The IRF was determined using scattered light at the excitation wavelength from a ludox sample. The absorbance of the fluorophores in all solutions at the excitation wavelength was near 0.1. The steady-state intensities of the samples were found to be stable during the lifetime measurements.

4.3 Femtosecond Transient Absorption (fsTA)

fsTA experiments were performed with a Spectra-Physics Hurricane Titanium:Sapphire regenerative amplifier system. The 488 nm pump pulse was generated using an optical parametric amplifier (Spectra-Physics OPA 800C). Residual 800 nm light was focussed on a sapphire plate to produce white probe light which was detected with a charge-coupled device detector (Ocean Optics). The polarization of the pump beam was at the magic angle (54.7°) with respect to that of the probe (Berek Polarization Compensator (New Focus)). The excitation pulse was passed over an optical delay line (Physik Instrumente, M-531DD) that generated an experimental time window of up to 3.6 ns between the excitation and probe pulses with a maximal resolution of 0.6 fs/ step. The laser output was typically ~2 μJ pulse⁻¹ (130 fs FWHW) with a repetition rate of 1 kHz. The samples were placed in cells of 2 mm path length (Hellma) and stirred with a downward projected PTFE shaft using a direct drive spectro-stir (SPECTRO-CELL). Data were analyzed using Glotaran software.⁷

4.4 Additional spectra and fluorescence decay curves

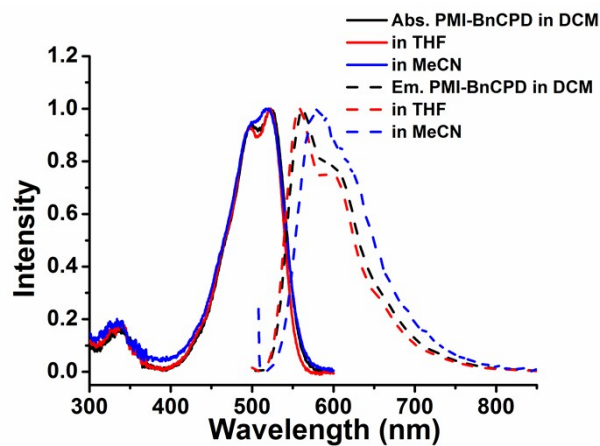


Fig. S2 Static absorption and emission spectra of **PMI-BnCPD 1** in various solvents (DCM, THF and MeCN).

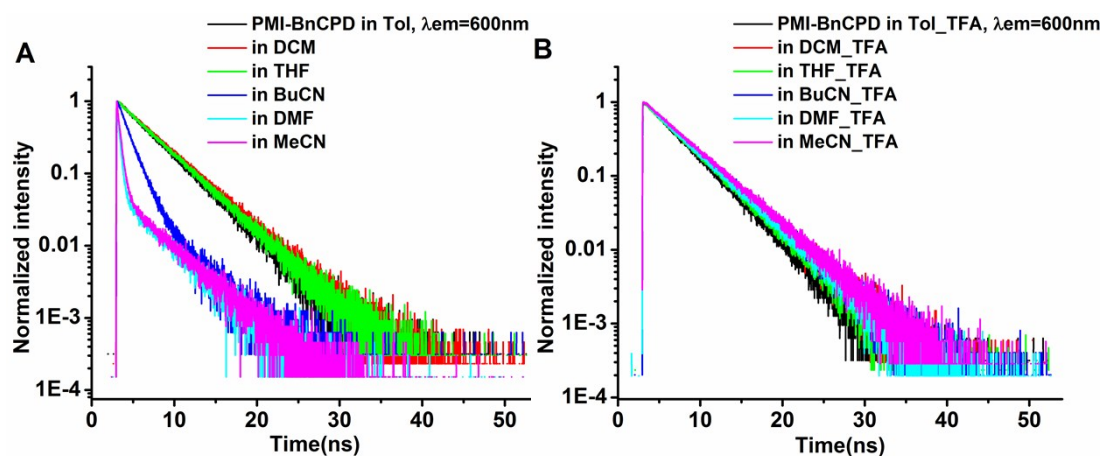


Fig. S3 Fluorescence decay curves of **PMI-BnCPD 1** in six different solvents with (B) and without (A) TFA at $\lambda_{\text{ex}} = 488 \text{ nm}$, $\lambda_{\text{em}} = 600 \text{ nm}$.

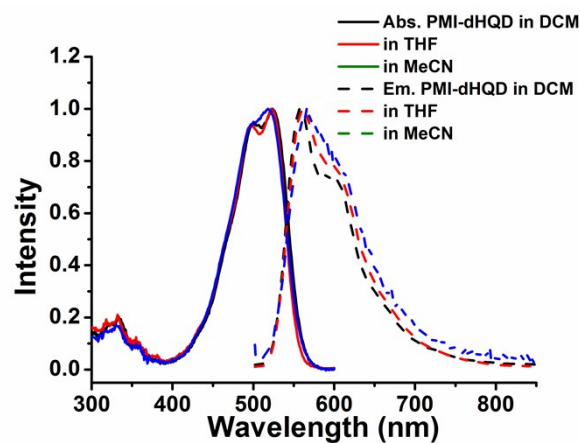


Fig. S4 Static absorption and emission spectra of **PMI-dHQD 2** in different solvents (DCM, THF and MeCN).

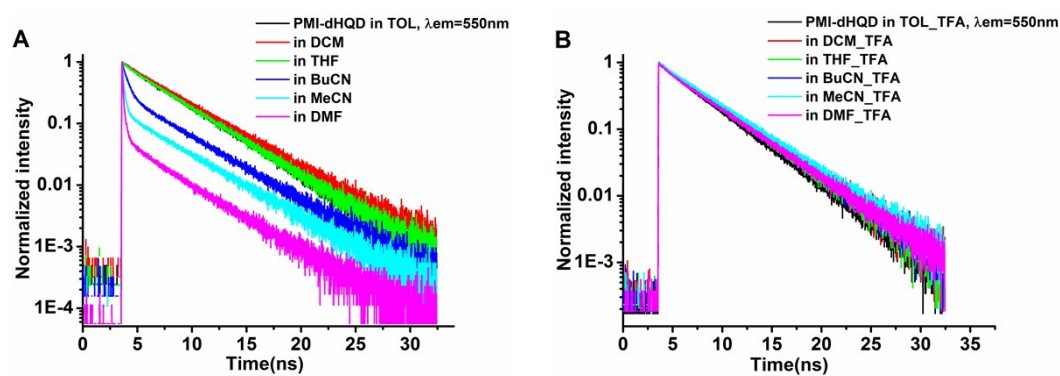


Fig. S5 Fluorescence decay curve of **PMI-dHQD 2** in six different solvents with (B) and without (A) TFA at $\lambda_{ex} = 488$ nm, $\lambda_{em} = 550$ nm.

Table S1 Fluorescence decay times of **PMI-BnCPD 1** and **PMI-dHQD 2** in different solvents with and without TFA acid at $\lambda_{\text{ex}} = 488 \text{ nm}$, $\lambda_{\text{em}} = 550 \text{ nm}$.

Compound	Solvent	Dielectric constant	τ_1 (ns)/ Amp. (%)	τ_2 (ns)/ Amp. (%)	Reduced Chi ²
PMI-BnCPD 1	TOL	2.38	3.85/ 100		1.11
	+TFA		3.82/ 100		1.08
	DCM	9.1	4.25/ 100		1.09
	+TFA		4.24/ 100		1.04
	THF	7.5	4.04/ 100		1.16
	+TFA		4.06/ 100		1.10
	BuCN	20.7	4.35/ 3	1.27/ 97	1.09
	+TFA		4.10/ 100		1.12
	MeCN	37.5	3.99/ 1	0.38/ 99	1.09
	+TFA		4.43/ 100		1.07
PMI-dHQD 2	DMF	38	3.77/ 2	0.25/ 98	1.13
	+TFA		4.17/ 100		1.17
	TOL	2.38	3.87/ 100		1.11
	+TFA		3.85/ 100		1.11
	DCM	9.1	4.21/ 100		1.14
	+TFA		4.23/ 100		1.12
	THF	7.5	3.88/ 100		1.17
	+TFA		4.08/ 100		1.13
	BuCN	20.7	4.17/ 3	0.48/ 97	1.02
	+TFA		4.18/ 100		1.18
MeCN	37.5	4.14/ 1	0.15/ 99	1.11	
+TFA		4.41/ 100		1.10	
DMF	38	3.70/ 2	0.10/ 98	1.13	
+TFA		4.17/ 100		1.17	

5 Cyclic voltammogram of quinuclidine, the model electron donor

The cyclic voltammograms was recorded on a Zahner ZENNIUM electrochemical workstation with a conventional three-electrode system with a homemade Ag/AgCl electrode as a reference electrode, a platinum wire with 0.5 mm diameter as a counter electrode, and a glassy carbon electrode as a working electrode. The measurements were performed at room temperature on solutions in nitrogen purged butyronitrile with tetrabutylammonium hexafluoro-phosphate (TBAH, 0.1 M) as the supporting electrolyte.

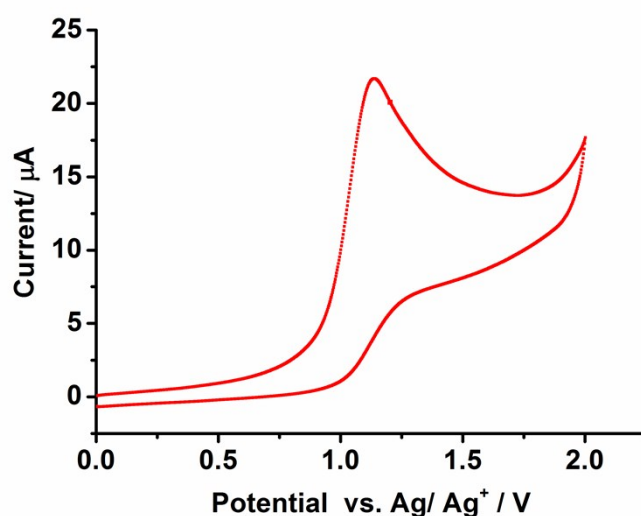


Fig. S6 Cyclic voltammograms of quinuclidine (1 mM) in butyronitrile with 0.1 M TBAH, scan rate 100 mV/s.

6 Additional fsTA spectra

An alternative explanation for the fast spectral shift at early times could be the transition from the LE state to the CT state. To test this, trifluoroacetic acid (TFA) was added to the polar solvent, which prevents the intramolecular CT of compound **1** by protonating the quinuclidine donor. The ESA in **Fig. S7** show that TFA does not remove the fast spectral shift process, so we can exclude that charge separation is **not** the cause.

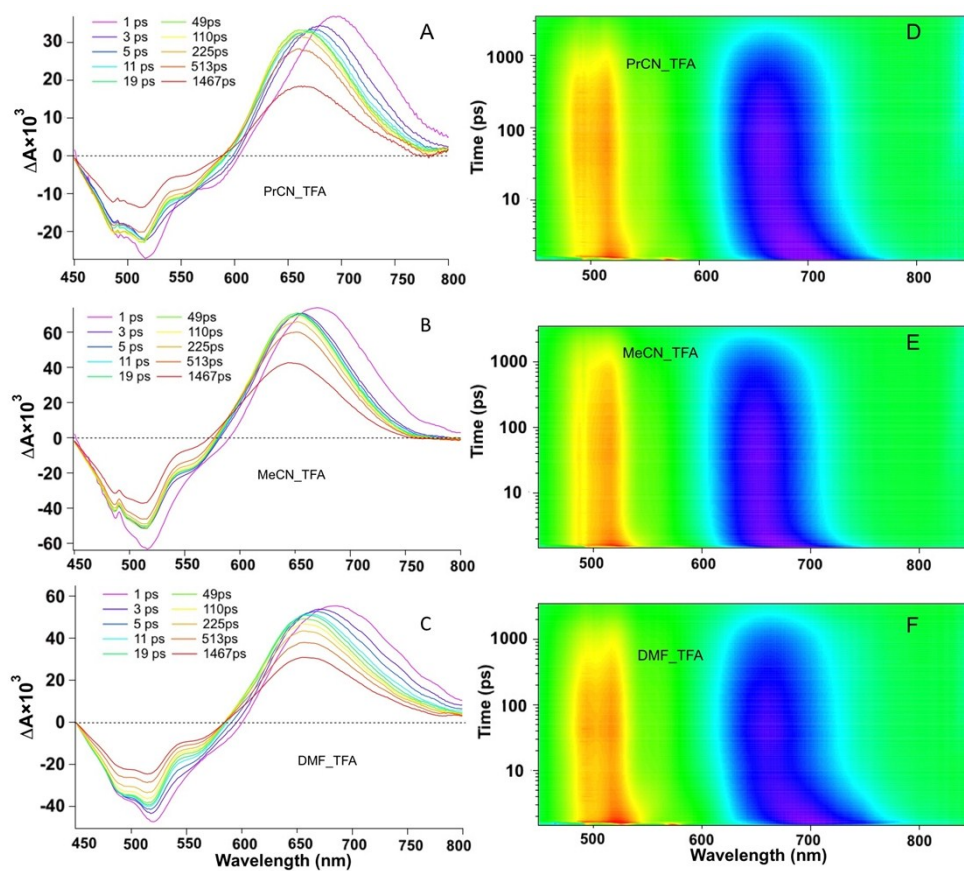


Fig. S7 fs-TA spectra obtained for **PMI-BnCPD** at the specified time delays in the 3 polar solvents (PrCN, MeCN and DMF) with TFA acid mixtures indicated after photo-excitation at 488 nm at room temperature.

7 Conformational analysis

The large conformational space available to compounds **1** and **2** prohibits a thorough conformational analysis within the context of our experimental study. In order to find representative low-energy structures we first performed a conformational search using molecular mechanics (Macromodel program, MM3 force field, CHCl₃ solvent model) and then minimized the energies of the lowest-energy conformers (20 kJ/mol window for the MM3 energy) using a standard DFT approach (B3LYP functional; 6-31G(d) basis set, Polarizable Continuum Model with CHCl₃ as the solvent; Gaussian 09 (revision D.1⁸)). For PMI-dHQD we found 18 conformations within an energy window of 10 kJ/mol. For PMI-BnCPD **1** there were 32. This energy window is smaller than the potential error of the computed relative energies, but at least this approach allows us to find some representative low-energy structures.

The conformations of cinchona alkaloids are described in terms of two dihedral angles: N-C8-C9-C4' (anti vs. syn) and O-C9-C4'-C9' (open vs. closed). For PMI-dHQD the lowest energy structures belong to the “anti-open” class, but the other types are also found among the 18 lowest energy conformers. Further conspicuous differences are in the orientation of the 9-OH group and the 6'-OMe, and in the rotational angles of the PMI unit along the linear connection to the quinuclidine. In the case of PMI-BnCPD syn-closed and anti-open conformers predominate among the lowest-energy conformers, but the other types also appear within the 10 kJ/mol energy window.

We performed the same calculations with the ω B97XD functional, with very similar results.

In figure S8 we show the structure of the lowest-energy conformer, and the HOMO and LUMO orbitals. While the LUMO is localized on the PMI unit, the HOMO contains a substantial contribution from the quinuclidine nitrogen lone pair, coupled through the sigma bonds with the conjugated system.

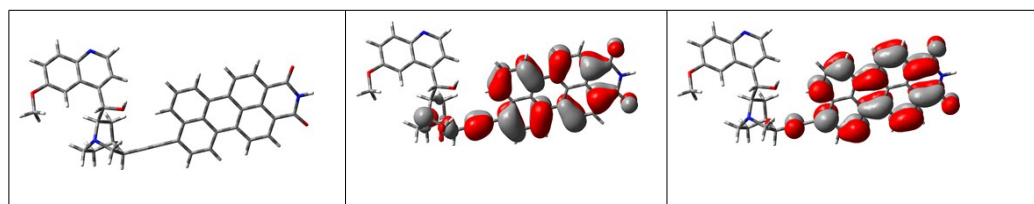


Fig. S8 Lowest-energy structure (B3LYP/6-31G(d)) for **2**, and HOMO and LUMO orbitals.

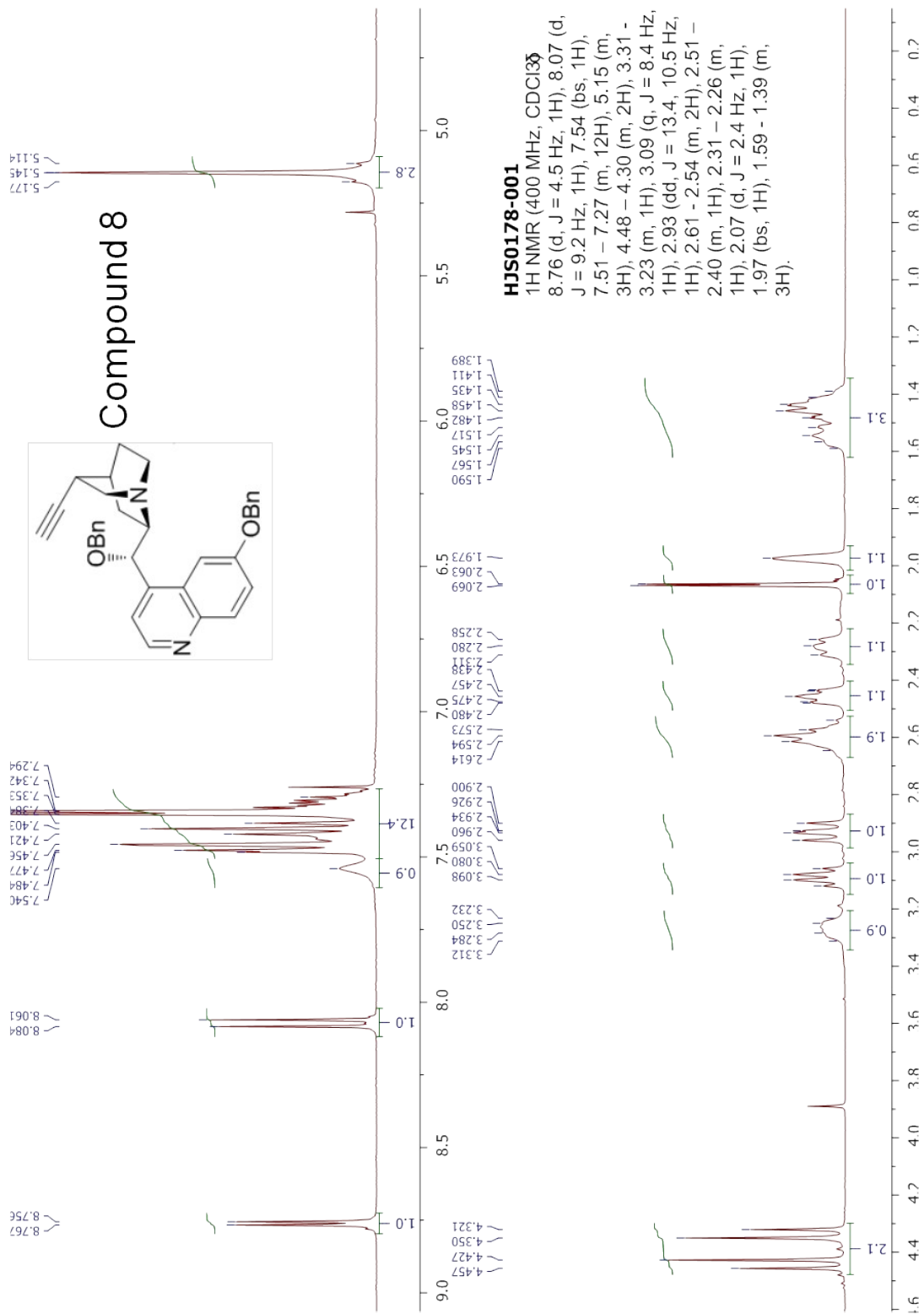


Fig. S10 ¹H NMR spectra of compound **8** in CDCl₃.

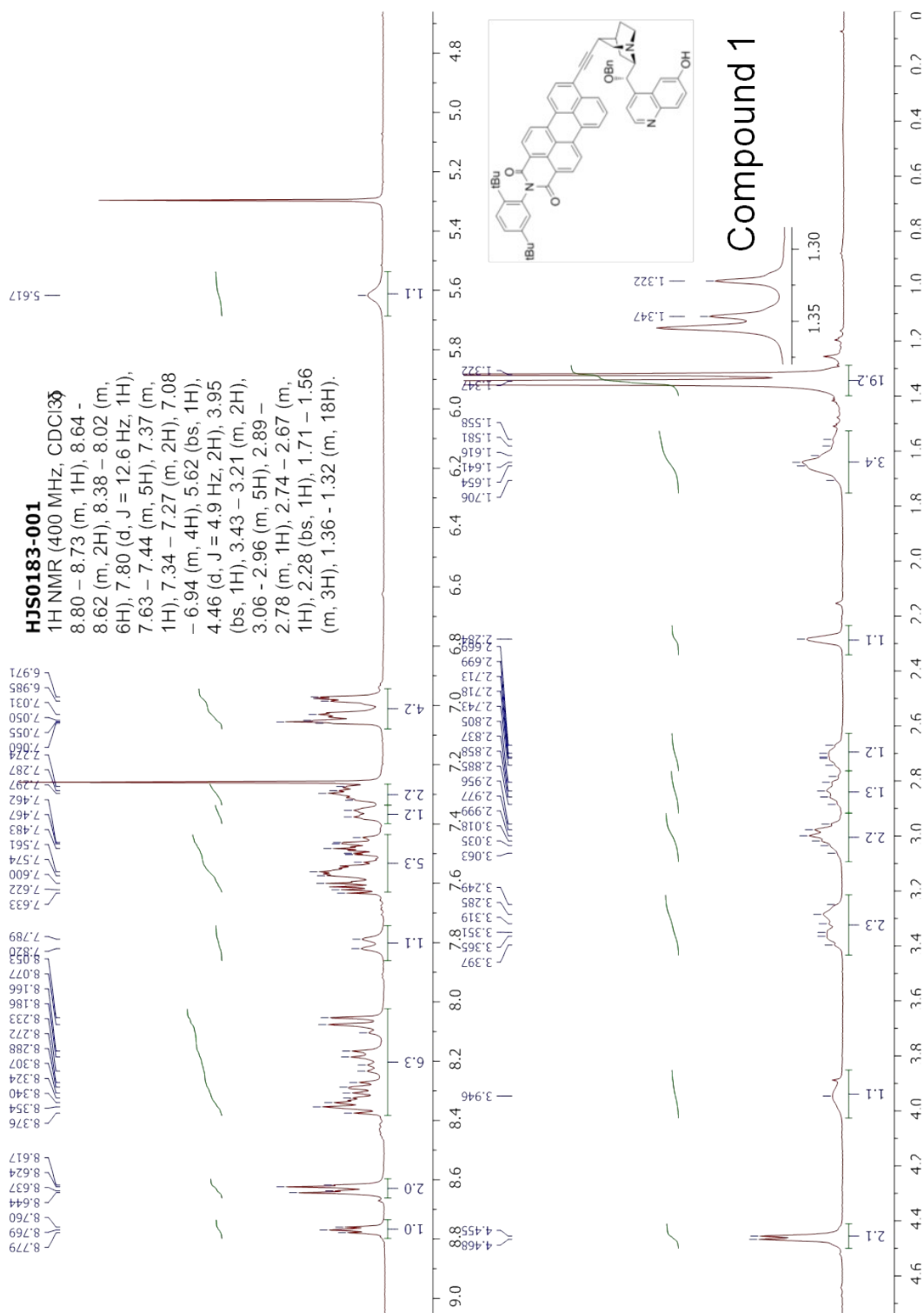


Fig. S13 ¹H NMR spectra of compound **1** in CDCl₃

9 LCMS analysis of compound 1

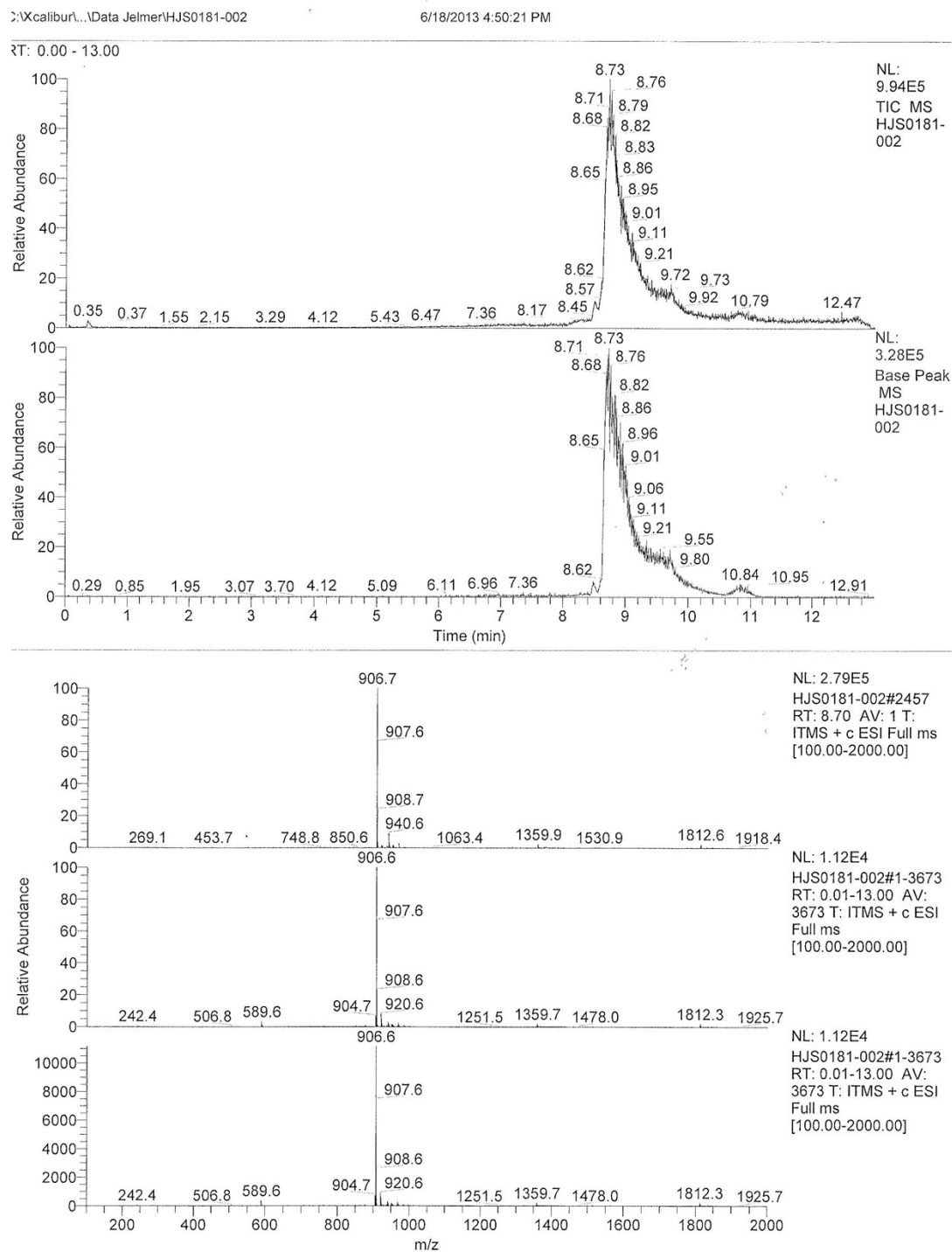


Fig. S14 LCMS of compound 1. Solvent and mobile phase MeCN:H₂O = 1:1.

10 References

1. T. Marcelli, Cinchona-derived Organocatalysts for Asymmetric Carbon–Carbon Bond Formation, PhD thesis, Universiteit van Amsterdam, 2007.
2. T. Gessner, H. Reichelt, I. Münster, M. Könemann, N. G. Pschirer, J. Qu, R. Sens, A. Schwögler and A. Manetto, US Patent US8802852B2, 2014.
3. T. Matsumoto, Y. Urano, T. Shoda, H. Kojima and T. Nagano, *Org. Lett.*, 2007, **9**, 3375-3377.
4. T. Kumpulainen and A. M. Brouwer, *Phys. Chem. Chem. Phys.*, 2012, **14**, 13019-13026.
5. H. Lehtivuori, A. Efimov, H. Lemmetyinen and N. V. Tkachenko, *Chem. Phys. Lett.*, 2007, **437**, 238-242.
6. H. Lehtivuori, T. Kumpulainen, A. Efimov, H. Lemmetyinen, A. Kira, H. Imahori and N. V. Tkachenko, *J. Phys. Chem. C*, 2008, **112**, 9896-9902.
7. J. J. Snellenburg, S. P. Laptanok, R. Seger, K. M. Mullen, and I. H. M. van Stokkum, *J. Stat. Softw.* 2012, **49**, 1-22.
8. Gaussian 09, Revision D.01, M. J. Frisch, G. W. Trucks, H. B. Schlegel, G. E. Scuseria, M. A. Robb, J. R. Cheeseman, G. Scalmani, V. Barone, B. Mennucci, G. A. Petersson, H. Nakatsuji, M. Caricato, X. Li, H. P. Hratchian, A. F. Izmaylov, J. Bloino, G. Zheng, J. L. Sonnenberg, M. Hada, M. Ehara, K. Toyota, R. Fukuda, J. Hasegawa, M. Ishida, T. Nakajima, Y. Honda, O. Kitao, H. Nakai, T. Vreven, J. A. Montgomery, Jr., J. E. Peralta, F. Ogliaro, M. Bearpark, J. J. Heyd, E. Brothers, K. N. Kudin, V. N. Staroverov, T. Keith, R. Kobayashi, J. Normand, K. Raghavachari, A. Rendell, J. C. Burant, S. S. Iyengar, J. Tomasi, M. Cossi, N. Rega, J. M. Millam, M. Klene, J. E. Knox, J. B. Cross, V. Bakken, C. Adamo, J. Jaramillo, R. Gomperts, R. E. Stratmann, O. Yazyev, A. J. Austin, R. Cammi, C. Pomelli, J. W. Ochterski, R. L. Martin, K. Morokuma, V. G. Zakrzewski, G. A. Voth, P. Salvador, J. J. Dannenberg, S. Dapprich, A. D. Daniels, O. Farkas, J. B. Foresman, J. V. Ortiz, J. Cioslowski, and D. J. Fox, Gaussian, Inc., Wallingford CT, 2013.